Joint estimation of dynamic polarization and carrier phase with pilot-based adaptive equalizer in PDM-64 QAM transmission system

JIAQIAN YANG,* Eric Sillekens, Wenting Yi, Polina Bayvel, AND Robert I. Killey

Optical Networks Group, Department of Electronic and Electrical Engineering, UCL, London, WC1E 7JE, UK

*jiaqian.yang.18@ucl.ac.uk

Abstract: A pilot-based adaptive equalizer is investigated for high cardinality polarization-division-multiplexing quadrature amplitude modulation transmission systems. Pilot symbols are periodically inserted for joint estimation of the dynamic state of polarization (SOP) and carrier phase, in a least mean square (LMS) sense. Compared to decision-directed least mean square (DDLMS) equalization and radially-directed equalization, the proposed equalizer can achieve robust equalization and phase estimation, especially in low optical signal-to-noise ratio (OSNR) scenarios. In an experiment on 56 GBaud PDM-64 QAM transmission over 400 km standard single-mode fiber, we obtained at least 0.35 bit per symbol generalized mutual information (GMI) improvement compared with other training symbol-based equalization when tracking 600 krad/s dynamic SOP. With the joint estimation scheme, the equalization performance will not be compromised even if the SOP speed reaches 600 krad/s or the laser linewidth approaches 2 MHz. For the first time, it is demonstrated that the pilot-based equalizer can track dynamic SOP rotation and compensate for fiber linear impairments without any cycle slips under extreme conditions.

1. Introduction

In metro and long-haul fiber links, the requirement to reliably transmit high speed data has stimulated the evolution of wide band optical transmission systems. Polarization division multiplexing (PDM) coherent transceivers have attracted intensive research [1–4] due to the high spectral efficiency they offer, and digital signal processing (DSP) has been used in such systems for over a decade, enabling the mitigation of a variety of impairments, including laser phase noise (PN), chromatic dispersion (CD), polarization mode dispersion (PMD), and fast state of polarization (SOP) change [5–11]. However, conventional blind DSP approaches [12–14] will encounter a limitation where the equalization may be unable to converge due to the ultrafast rate of change of SOP of up to 5.1 Mrad/s [15] caused by lightning strikes and mechanical vibrations [15–17] or the cycle slip in phase estimation. Several tracking algorithms have been proposed recently including Kalman filter, training symbol-based channel estimator and nonlinear principle component analysis [18–21], but they are either sensitive to amplified spontaneous emission (ASE) noise or unable to mitigate the intersymbol interference (ISI).

In this paper, we propose a pilot-based multiple-input multiple-output (MIMO) equalizer where pilots are used for joint adaptive equalization and carrier phase estimation (CPE), which can mitigate the PMD effects and achieve a reliable tracking of the fast dynamic SOP change that may occur in modern transmission systems. With the help of pilot symbols, this equalization algorithm can achieve similar or even better performance with lower complexity compared to previous methods due to fewer updates of the filters. Unlike the decision-directed least mean square

(DDLMS) [13,14] or other proposed data-aided equalization algorithms [22,23], we introduce the pilot symbols for two purposes: by comparing the pilot and the recovered signal, the carrier phase is estimated directly in the equalization process without requiring the decision-directed digital phase locked loop (DPLL). The aim of this step is to prevent the adaptive equalizer (AEQ) from being affected by the fast phase fluctuation and to reduce latency during the adaptive operation compared with decision-directed algorithms or frequency domain equalization [24]. On the other hand, the replacement of the decision symbols in the error function by the pilot ones provides more certainty in the error calculation and makes the equalizer less affected by the ASE noise. In addition, the pilot-based equalizer enables the avoidance of decision-making during the DSP and is thus immune to cycle slips, which can be a limiting factor in the performance of blind algorithms. In pilot-based equalization which is capable of mitigating all linear impairments in fiber transmission, our method achieves at least 0.35 bit/symbol higher information rate when tracking 600 krad/s rotation of SOP (RSOP) in PDM-64 QAM transmission. The simulation and experiment results show that the proposed AEQ outperforms blind [12] or other pilot-based algorithms [23] and can work without significant loss of generalized mutual information (GMI) at SOP speed of 600 krad/s and laser linewidth of 2 MHz in 56 GBaud 64 QAM systems.

2. Principle of pilot-based DSP

2.1. Pilot-based equalization

To compensate for the polarization effects, a group of finite impulse response (FIR) filters in a MIMO structure are often employed. The update algorithm is described by Eq. (12)–(19) in [5] where the cost function is calculated in a mean squares sense and the error criteria are constant modulus followed by DDLMS. This blind scheme can achieve a high throughput in cases of high optical signal-to-noise ratio (OSNR), due to the accurate symbol decisions and negligible symbol errors. As the OSNR decreases, however, the decision device becomes more likely to categorize the symbols incorrectly because both the received and recovered symbols are affected by the ASE noise. Consequently, the equalizer will either give a rotated constellation with unpredictable cycle slip or completely fail to recover the transmitted symbols.

To avoid this failure, we propose a pilot-based equalizer where the pilot symbols are periodically inserted into the payload and transmitted together. In this case, no matter how severely the symbol is affected by the ASE noise, as long as the cross correlation-based frame synchronization can give a relatively accurate delay estimation, which is possible with the pre-equalization technique in our experiments, prior information of the transmitted symbol at the pilot position is always available at the receiver end. Assuming the pilot insertion rate is $1/N_s$ (see Fig. 1) and the pilot symbols at time $N_s k$ is $x_p(N_s k)$ and $y_p(N_s k)$, the error function becomes:

$$\epsilon_x = x_p(N_s k) - x_{\text{out}} \tag{1}$$

$$\epsilon_y = y_p(N_s k) - y_{\text{out}} \tag{2}$$

where x_{out} and y_{out} denote the equalizer outputs at time $N_s k$. These error calculations no longer rely on the hard decision of the received symbols after equalization and CPE; instead, transmitted pilot symbols which are known at the receiver can be used, and the computational complexity can be reduced as well. The update functions remain the same:

$$\mathbf{h}_{xx} \rightarrow \mathbf{h}_{xx} + 2\mu \epsilon_x^* \mathbf{x}_{\text{in}} \tag{3}$$

$$\mathbf{h}_{xy} \rightarrow \mathbf{h}_{xy} + 2\mu \epsilon_x^* \mathbf{y}_{\text{in}} \tag{4}$$

$$\mathbf{h}_{yx} \rightarrow \mathbf{h}_{yx} + 2\mu \epsilon_y^* \mathbf{x}_{\text{in}} \tag{5}$$

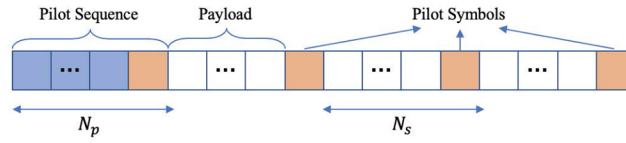$$\mathbf{h}_{yy} \rightarrow \mathbf{h}_{yy} + 2\mu \epsilon_y^* \mathbf{y}_{\text{in}} \tag{6}$$

Fig. 1. Data frame with inserted pilot sequence and pilot symbols. The insertion rate is $1/N_s$ and the length of the pilot sequence is N_p.

Here, the filter taps **h** is a complex-valued vector with filter length L, μ is the learning rate, $*$ denotes complex conjugate, $\mathbf{x}_{\text{in}}$ and $\mathbf{y}_{\text{in}}$ are the received symbol vectors: $\mathbf{x}_{\text{in}}(k) = [x_{\text{in}}(k), x_{\text{in}}(k-1), \ldots, x_{\text{in}}(k-L+1)]^{\text{T}}$, $\mathbf{y}_{\text{in}}(k) = [y_{\text{in}}(k), y_{\text{in}}(k-1), \ldots, y_{\text{in}}(k-L+1)]^{\text{T}}$, the superscript T denotes the vector transpose.

2.2. Data frame construction

To guarantee a fast convergence of the above pilot-based equalization, we applied the recursive least square (RLS) algorithm at the beginning of the equalization. This leads to the construction of the data frame as shown in Fig. 1.

At the transmitter, a pilot sequence of length N_p is inserted at the beginning of the symbol stream, followed by equally-spaced pilot symbols with a pilot rate of $1/N_s$. Since the pilot symbols will be used not only in the equalization but also in CPE, which will be explained in Section 2.3, both pilot sequence and pilot symbols are quadrature phase shift keying (QPSK) symbols in order to maximize the symbol modulus (in the sense of normalized power), and thus increasing the accuracy of phase estimation.

After the compensation of chromatic dispersion at the coherent receiver, the proposed pilot-based equalizer is applied. The MIMO filters are initialized by the pilot sequence using the RLS algorithm to guarantee a fast convergence. The principle of RLS can be found in [25] and will not be explained in this paper, but the simulation parameters will be listed in Section 3. Then, the equalizer turns to LMS based on the following equally spaced pilot symbols using Eq. (1)–(6) and starts to track the RSOP and to mitigate the polarization effects. The simulation result will show that once our pilot-based equalizer converges, it can continuously track the RSOP and the data frame length will no longer be limited by the DSP algorithms. In real implementations, however, the memory of the hardware should also be considered when designing the data frame length.

2.3. Joint equalization and CPE

To recover the received symbols correctly and robustly under low OSNR and high PN conditions, we propose the joint equalization and CPE scheme. Unlike the pilot-based DSP described in [22,23] in which the pilot symbols are only used for CPE, or where the two-step DSP is carried out separately (CPE after equalization), our proposed scheme uses the pilot symbols to estimate the carrier phase during the equalization, and the estimated phase in turn helps to modify the error function in the equalization.

A comparison between the conventional DSP and the proposed scheme is shown in Fig. 2. In the conventional blind AEQ based on the constant modulus algorithm (CMA) or DDLMS, the AEQ is updated at each symbol with the error calculated directly from the equalizer outputs or after phase recovery. Taking the x-polarization signal for example, the output of the equalizer is:

$$x_{\text{out}}(k) = \mathbf{h}_{xx}^{\text{H}} \mathbf{x}_{\text{in}}(k) + \mathbf{h}_{xy}^{\text{H}} \mathbf{y}_{\text{in}}(k) \tag{7}$$

The superscript H indicates the complex conjugate transpose and $\mathbf{x}_{\text{in}}(k)$, $\mathbf{y}_{\text{in}}(k)$ are the input vectors defined in Section 2.1. The error is calculated with CMA or DDLMS criteria, respectively:
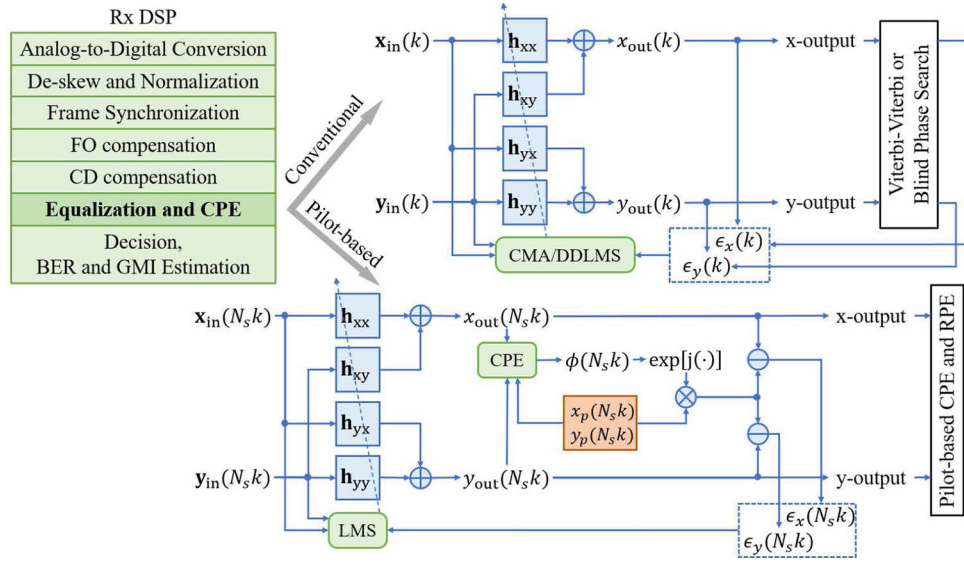
$$\epsilon_x(k) = 1 - |x_{\text{out}}(k)|^2 \tag{8}$$

Fig. 2. Comparison between conventional receiver DSP and pilot-based DSP. (**h**: AEQ filter tap weights. ϵ: error function. x_p, y_p: pilot symbols. ϕ: estimated carrier phase. FO: frequency offset; CD: chromatic dispersion; CPE: carrier phase estimation; RPE: residual phase estimation.)

$$\epsilon_x(k) = d_x(k) - \hat{x}_{\text{out}}(k) \tag{9}$$

Here, "1" denotes the constant modulus. If radially-directed equalizer (RDE) is applied, the "1" is substituted by the closest multi-level modulus. $\hat{x}_{\text{out}}(k)$ represents the x-output after phase recovery, and $d_x(k)$ is the symbol closest to $\hat{x}_{\text{out}}(k)$. Then the CMA/RDE or DDLMS filter updating rules apply at each symbol, respectively:

$$\mathbf{h}_{xx} \rightarrow \mathbf{h}_{xx} + \mu\epsilon_x(k)x_{\text{out}}^*(k)\mathbf{x}_{\text{in}}(k) \tag{10}$$

$$\mathbf{h}_{xx} \rightarrow \mathbf{h}_{xx} + 2\mu\epsilon_x^*(k)\mathbf{x}_{\text{in}}(k) \tag{11}$$

As can be seen, the CMA/RDE error in Eq. (8) will not be affected by the phase term, but the signal which is corrupted by the ASE noise is still unable to maintain the constant modulus or multi-level modulus property in low OSNR cases. Thus, the performance of the CMA/RDE will be significantly impaired, as cycle slips are more likely to occur in the blind CPE. This is why we introduce the pilot-based equalization as explained in Section 2.1. In Eq. (9), the error calculation takes its input from the phase estimation result and will induce additional delay associated with the CPE and decision devices. To better model what the signal experiences in the channel and avoid the necessity of making decisions in updating the equalizer and in the CPE which may lead to incorrect categorization in the presence of noise, we propose a novel pilot-based AEQ with joint equalization and CPE structure as illustrated in the lower part of Fig. 2.

The main principle of the joint equalization and CPE lies in estimating the laser phase with pilot symbols during the equalization process and using the phase to modify the error and update Eq. (1)–(6). With this scheme, the laser PN is estimated in each iteration and can be removed in the error calculation, which will not affect the performance of the equalization. This significantly improves the AEQ's tolerance to severe PN. To simplify the DSP, the CPE block in Fig. 2 operates as follows: comparing the pilot symbols x_p, y_p with the equalized symbols $x_{\text{out}}, y_{\text{out}}$ to obtain the phase angle and taking the mean value of adjacent phase angles to obtain the estimated PN. It should be noted that this CPE block is a coarse estimation of the PN and the main aim is to

reduce the influence of PN on the AEQ. More accurate CPE will be implemented in two steps (pilot-based CPE and residual phase estimation) after equalization.

Another feature of the proposed scheme is the ability to reduce the AEQ complexity. In contrast to conventional equalizers which update the filters at each symbol to achieve the best dynamic tracking result, the pilot-based equalizer only updates at pilot symbol position and the new tap weights are used for all the following payloads until the next pilot. This reduces the calculation complexity by a factor of N_s. The simulation and experiment results will show that the proposed algorithm can achieve similar or even better results with reduced complexity.

The detailed joint equalization and CPE operation of the pilot-based MIMO equalizer is as follows: assuming the PN ϕ_0 has negligible change at the beginning of the transmission and the RLS will bring the AEQ to a convergence with the help of the pilot sequence, then, at each pilot symbol position $N_s k$, the CPE block uses the pilot symbols $x_p(N_s k), y_p(N_s k)$ and recovered symbols $x_{\text{out}}(N_s k), y_{\text{out}}(N_s k)$ to estimate the current phase $\phi(N_s k)$. Note that this phase could be different from the real phase noise by ϕ_0 because the converged filter taps after RLS have already calibrated the phase term in the initial stage. Then, the phase is used to modify the error function Eq. (1)–(2) [13,14]:

$$\epsilon_x(N_s k) = x_p(N_s k) \exp[j\phi(N_s k)] - x_{\text{out}} \tag{12}$$

$$\epsilon_y(N_s k) = y_p(N_s k) \exp[j\phi(N_s k)] - y_{\text{out}} \tag{13}$$

Note that we assume a common phase for both polarization states and the pilot symbol is now rotated by a phase angle $\phi(N_s k)$ to eliminate the effect of PN. In other words, the ideal output of the equalizer is no longer the exact constellation point but the pilot symbol with the estimated phase noise added. Finally, we apply the LMS updating rules in Eq. (3)–(6) and the updated tap weights are used for the following payload symbols as well. Once this process converges, the AEQ can continuously track the RSOP throughout the symbol stream with the filters only modified at pilot symbol positions, corresponding to $1/N_s$ calculation complexity. Since the AEQ only updates at the QPSK pilot symbols, the modulation format of the payload can be chosen arbitrarily, and the proposed scheme is easily extended to any m-QAM modulation systems. Moreover, we found that, in 56 GBaud transmission, with the joint equalization and CPE scheme, the proposed AEQ can operate without significant loss of GMI in extreme conditions (fast RSOP of 600 krad/s and broad laser linewidth of 2 MHz) with only 4.64% overhead (i.e., at $1/N_s = 1/32$ and $N_p = 1024$) and does not diverge even if the OSNR is reduced to 26dB.

The last operation in the receiver DSP is the accurate phase recovery which is split into two steps. The first step is using the pilot symbols to estimate the moving mean value of the PN and to interpolate between pilots with spline interpolation. Then the PN is filtered by a finite impulse response (FIR) Wiener filter which models and recovers the random walk property of PN [26]. If the pilot interval N_s is sufficiently small, the interpolation and Wiener filter can effectively compensate for the PN. Unlike the blind CPE algorithms which require decision-making, such as DPLL and BPS, the pilot-based CPE only relies on the deterministic pilot symbols to estimate the phase and is thus immune to cycle slip. In the case of severe PN, we introduce the second step of PN compensation after down-sampling, which is called residual phase estimation (RPE) based on the maximum likelihood algorithm [27]. Finally, the recovered symbols are de-mapped and the bit error rate (BER) and GMI are calculated on the payload symbols.

3. Simulation results

A 56 GBaud PDM-64 QAM coherent transceiver was investigated through numerical simulations and the DSP was operated at two samples per symbol. A random input sequence of 2^{16} symbols was transmitted on both polarizations, where the first $N_p = 1024$ symbols form a pilot sequence and the following pilot symbols are inserted at the pilot rate of $1/N_s = 1/32$, corresponding to 4.64% overhead. The impact of the pilot insertion rate on the tolerance of the RSOP tracking

speed and the laser linewidth should be considered when choosing the value of N_p and N_s. Since the updating of the AEQ only takes place at pilot symbol position, the performance of the AEQ would remain the same if the pilot insertion rate and RSOP speed increase or decrease by the same percentage. A similar principle applies to the impact of pilot insertion rate on the system's tolerance to laser linewidth. We applied the frame structure used in [28] in the remainder of this paper, mainly aiming to handle RSOP speeds of up to 600 krad/s and 2 MHz laser linewidth.

At the transmitter, the symbols on both polarizations were pulse shaped by a root-raised-cosine (RRC) filter with 0.01 roll-off factor before being modulated using an ideal dual polarization (DP) in-phase/quadrature (I/Q) modulator driven by 91GSa/s 8-bit DAC. In the following, the laser linewidth was set to 100 kHz if not otherwise specified. The non-zero linewidth adds a random phase noise $\phi(k)$ to the transmitted signal. The phase term $\phi(k)$ usually follows a random walk with a variance proportional to the laser linewidth [29]. Since the fiber nonlinearity was not considered in the simulation and the OSNR was adjusted before the reception, the signal launch power could be set to arbitrary value. In the following simulations, we chose −8 dBm and the received signal power was normalized before DSP.

The PDM-64 QAM transmission channel used in the simulation is shown in Fig. 3. Due to the short distance considered in this paper, the fiber nonlinearity was not included in the simulation. Regarding the dynamic RSOP, the commonly used polarization scrambling Jones matrix is the continuous SOP model with a constant rotation speed ω [5]:

$$\mathbf{J}_{SOP} = \begin{bmatrix} \cos(\omega k) & -\sin(\omega k) \\ \sin(\omega k) & \cos(\omega k) \end{bmatrix} \tag{14}$$
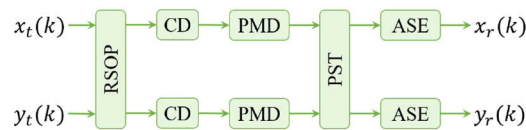

Fig. 3. Channel model of the coherent optical PDM-64 QAM transmission system. (RSOP: rotation of the state of polarization; CD: chromatic dispersion; PMD: polarization mode dispersion; PST: polarization state transformation, typically refers to the polarization rotation along the fiber; ASE: amplified spontaneous emission noise.)

This matrix leads to a circular contour on the Poincaré sphere. Note that the angle on the Poincaré sphere is two times the rotation angle of the Jones vector, hence, we calculated the mean SOP speed from the trajectory of the Stokes vector around the surface of the Poincaré sphere. Then the signal was transmitted through a standard single-mode fiber with a length of 80 km where the CD, PMD, and random polarization rotation effects were taken into account. The CD and PMD parameters were set to 17 ps/(nm · km) and 0.5 ps/$\sqrt{km}$, respectively, and the random polarization rotation angle took values from $(-\pi, \pi]$. As we mainly considered the dynamic property of RSOP using Eq. (14), we regarded the DGD as the only element in PMD simulation and took a constant mean value in the simulation. At the end of the transmission link, the ASE noise was added according to the system OSNR defined in a 0.1nm resolution bandwidth.

An ideal coherent detection with ADC sampling frequency being set to the same as DAC sampling frequency was considered, followed by ideal CD compensation and the proposed DSP. In real implementation, the alignment of the frame could be carried out by operating cross correlation on the pilot sequence and the received waveform, and frequency offset could be estimated using the pilot sequence [22,28] before the proposed adaptive equalizer was applied. The forgetting factor in the RLS algorithm was set to 0.999. Four half-symbol-spaced 21-tap adaptive filters were initialized by the RLS and turned to pilot-based LMS with a step size

of 0.001, and joint equalization and CPE were employed in the AEQ. Here, the filter length should be sufficiently long to fully compensate the PMD, and the RSOP tracking would not be affected by the differential group delay. The Wiener filter was applied to filter the estimated carrier phase after equalization, followed by the RPE to compensate the residual phase noise after down-sampling. The GMI was calculated on the recovered payload symbols after the AEQ had converged.

For comparison, we also simulated the conventional DDLMS, RDE, and another pilot-based method (separate equalization and CPE [23]) under the same system conditions. Since the blind DDLMS algorithm convergence is difficult to achieve, we also used the RLS at the beginning of the DSP to guarantee the convergence to get the best performance that DDLMS can achieve. Decision-directed DPLL [12] was used in DDLMS, and blind phase search (BPS) [30] or pilot-based CPE (depending on which one resulted in the highest GMI) was applied after RDE to recover the carrier phase. Regarding the pilot-based method described in [23], the researcher mainly used RDE on pilot symbols. Since the pilots are QPSK symbols, we tested CMA on the pilot symbols in the following simulations.

The error performance of the proposed algorithm, which indicates the correctness of the symbols recovered by the pilot-based AEQ, was tested in the simulation with 600 krad/s RSOP speed and 28 dB OSNR. The error vector magnitude (EVM) between the recovered and the transmitted symbols is shown in Fig. 4(a) together with the error in the initial RLS phase. For comparison, we also simulated the DDLMS algorithm and the EVM is compared in Fig. 4(b). The proposed algorithm converges rapidly after RLS is applied for about 50 symbols and successfully tracks the SOP state of the following symbols without cycle slip, giving an average EVM of 11.4 %. However, the DDLMS equalizer suffers from occasional cycle slips (after approximately 40 k symbols in this simulation) and is no longer able to keep track of the dynamic SOP and recover the symbols correctly.
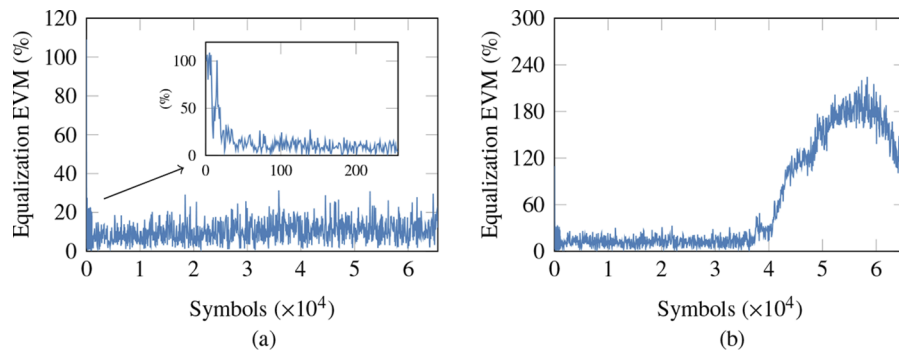

Fig. 4. Error vector magnitude of 64 QAM signal at 600 krad/s SOP rate and 28 dB OSNR with (a) proposed joint AEQ and CPE (inset: initial EVM with RLS algorithm), and (b) DDLMS.

A comparison of the error performance with three DSP algorithms is listed in Table 1. The proposed algorithm has a slightly higher EVM compared with DDLMS in high OSNR transmission, but the advantage is soon established as the OSNR decreases. Under 28 dB OSNR, the proposed algorithm outperforms the other algorithms with much smaller EVM when tracking 600 krad/s RSOP. In addition, the RDE failed to track dynamic RSOP at any OSNR, and pilot-based CMA can work with dynamic RSOP but with compromised performance. From the table, our proposed joint equalization and CPE scheme can achieve superior error performance and robust equalization under different OSNR. A detailed comparison is illustrated in Fig. 5.

Note that all the methods in the following simulations except DDLMS had pilot sequence and pilot symbols inserted, corresponding to 0.557 bit/4-D symbol capacity loss due to the
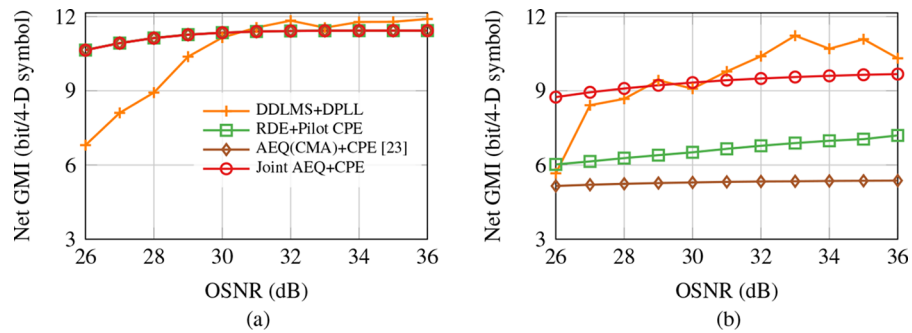
Fig. 5. Net GMI as a function of OSNR with different equalization and CPE algorithms in 56 GBaud 64 QAM transmission. (a) Static RSOP; (b) 1 Mrad/s RSOP.

Table 1. Comparison of the error performances.

DSP Algorithm	EVM (%)	
	OSNR = 36 dB	OSNR = 28 dB
DDLMS+DPLL	5.20	60.21
RDE+BPS	63.07	63.76
AEQ(CMA)+CPE [23]	18.09	19.46
Joint AEQ and CPE	8.79	11.4

pilot overhead. Therefore, we deducted the overhead and presented the net system GMI in the following results of comparison. When the SOP is static, all equalization methods achieve similar GMI except that DDLMS outperforms the others because of zero-overhead. However, DDLMS occasionally fails as the OSNR drops below 30 dB. As the RSOP speed increases to 1Mrad/s, DDLMS can still track the RSOP accurately, at the cost of updating the filters symbol by symbol, requiring high complexity. However, the fluctuation of the curve in Fig. 5(b) shows that, in some of the simulations, the system completely fails, giving a GMI of approximately zero, showing that DDLMS becomes unreliable in these cases. The other three algorithms exhibit different performance, with the proposed method giving approximately 3 bit/4-D symbol GMI improvement compared with the pilot-based CMA and the blind RDE.

To test the SOP tracking capability of the proposed algorithm, the SOP scrambling rate was varied from 1 krad/s to 1 Mrad/s and the test was performed under two different OSNRs. 100 tests were implemented for each SOP rate and the average GMI performances are presented in Fig. 6. Here, the DDLMS is updated symbol-by-symbol and can track RSOP 32 times faster than proposed algorithm in theory, making it the best method with superior RSOP tracking capability, as long as the system OSNR is sufficiently high, and the calculation complexity is not a major concern. However, the curve fluctuation in Fig. 6(b) indicates that, in many simulations, the system with DDLMS failed when the OSNR is low, and the averaged net GMI is no longer a reliable metric. The RDE performance is even worse at higher OSNR, due to the incorrect polarization alignment and the cycle slip. In contrast, the pilot-based methods show a smooth decreasing curve, and the algorithm can still work with an acceptable GMI loss (0.6 bit/symbol) when the RSOP speed increases to 600 krad/s. Note that the pre-convergence equalizer used in our proposed algorithm (mainly for frame synchronization) can limit the RSOP tracking performance, which could lead to some failed results. Even so, the proposed joint equalization and CPE still achieves approximately 3 bit/4-D symbol net GMI gain compared with other pilot-based method when the RSOP speed increases to 600 krad/s. In conclusion, our proposed algorithm has the most robust performance compared with the others and exhibits no significant

GMI loss when tracking the RSOP of approximately 600 krad/s. If greater RSOP speed tolerance is required in high OSNR transmissions, either DDLMS or the proposed AEQ with the more frequent insertion of pilot symbols could manage to track the ultrafast RSOP. Till now, this is the best dynamic SOP tracking result for PDM-64 QAM transmission by pilot-based AEQ which also compensates for the fiber PMD.
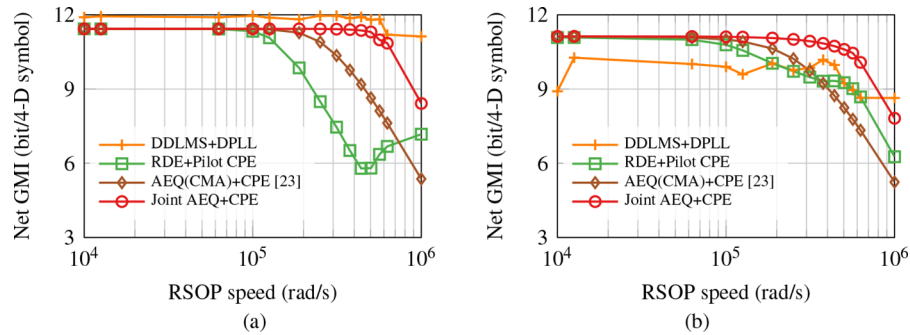

Fig. 6. Net GMI as a function of RSOP speed with different equalization and CPE algorithms in 56 GBaud 64 QAM transmission. (a) OSNR = 36 dB; (b) OSNR = 28 dB.

In some applications where low-cost lasers are desired for cost effective considerations, the laser linewidth becomes a limiting factor of the receiver DSP performance. Therefore, we further tested our algorithm under different laser linewidths, and the resulting GMI as a function of the linewidth-symbol duration product is plotted in Fig. 7. Since the joint equalization and CPE scheme is immune to cycle slip, and it automatically estimates the PN and takes the phase term into account in the error calculation, the proposed scheme becomes less affected by the severe PN during the equalization. This brings extra robustness of the algorithm with broad laser linewidth of greater than 1 MHz or severe PN. The RDE and the pilot-based CMA also perform well because the equalization is based on symbol modulus without considering phase noise, and the lower net GMI is attributed to their inability to dynamically track the RSOP. DDLMS completely fails as the laser linewidth increases to 1MHz, and the DPLL cannot calibrate the phase term anymore. As can be seen from Fig. 7, the proposed algorithm outperforms others when tracking 600 krad/s dynamic RSOP under 28 dB OSNR, and it can work even when $\Delta \nu T = 10^{-4}$, or equivalently, the
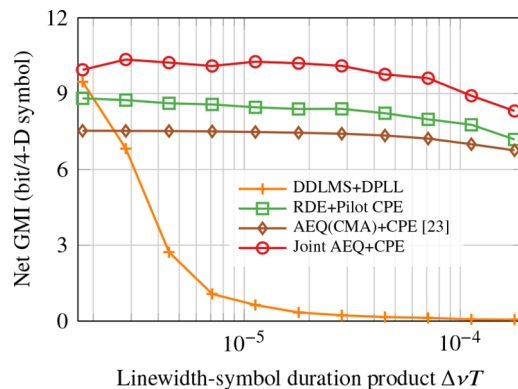

Fig. 7. Net GMI as a function of laser linewidth-symbol duration product with different equalization and CPE algorithms in 56 GBaud 64 QAM transmission. OSNR = 28 dB, RSOP speed = 600 krad/s.

laser linewidth approaches 10 MHz. In conclusion, our proposed joint equalization and CPE scheme has a robust RSOP tracking performance and is less affected by the laser linewidth.

4. Experimental results

A dual polarization (DP) 56 GBaud 64 QAM transmission system was tested. The experimental setup is shown in Fig. 8. An external cavity laser emitting at 1550 nm was modulated by a DP IQ modulator which was driven by 91 GSa/s 8-bit digital-to-analog converters (DACs). The modulated signal was amplified by an EDFA and followed by a variable optical attenuator (VOA) before being transmitted through a recirculating loop which was controlled by acousto-optic modulator (AOM) switches. The recirculating loop consisted of a polarization scrambler (PS), an 80 km standard single mode fiber (SSFM) span, a wavelength selective switch (WSS) and several EDFAs with noise figure of 5 dB and VOAs to control the signal power. The PMD and CD parameter of the SSFM was 0.5 ps/$\sqrt{\text{km}}$ and 16.72 ps/(nm · km), respectively. The output signal was coherently detected by a polarization-diverse optical 90-degree hybrid, four 70-GHz balanced photodetectors, and a digital sampling oscilloscope operating at 256 GSa/s. The captured signal was resampled to 2 samples per symbol before the offline DSP was carried out.
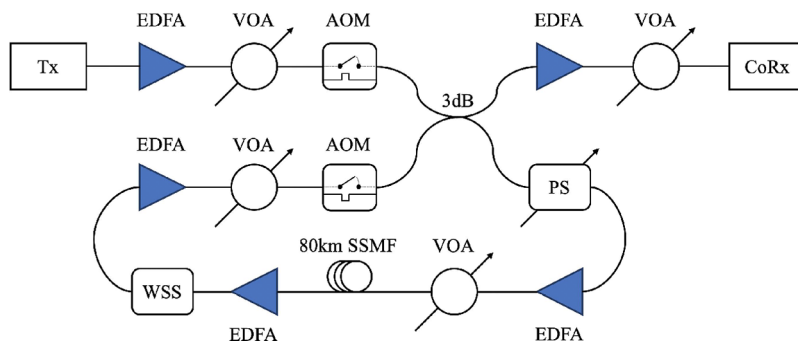

Fig. 8. Experimental setup of the DP 56 GBaud 64 QAM transmission system. VOA: variable optical attenuator. AOM: acousto-optic modulator. PS: polarization scrambler. SSMF: standard single mode fiber. WSS: wavelength selective switch.

After one recirculation of transmission (giving a transmission distance of 80 km), the received OSNR was measured by an optical spectrum analyzer and was approximately 28.6 dB. The PS was set to spinning mode in which the half-waveplate constantly rotated at a fixed speed and introduced dynamic RSOP to the link. The RSOP speed was varied from 0 to over 600krad/s which was the fastest speed that the PS could achieve. Different equalization and CPE algorithms were tested on the experimental data and the result is shown in Fig. 9(a). DDLMS achieves the highest net GMI because the FIR filters are updated at each symbol and there is no overhead in the data frame. The proposed algorithm has better performance compared with RDE and pilot-based CMA when tracking dynamic RSOP of greater than 100 krad/s. Compared with the simulation result in Fig. 6, the DAC frequency roll-off and digital pre-distorter impaired the received signal to some extent which was not considered in the simulation, so the net GMI obtained in the experiment is lower than the simulation by approximately 0.8 bit/4-D symbol.

We further transmitted the data through 5 recirculations, giving a total transmission distance of 400 km. The DSP result is shown in Fig. 9(b). In this case, the additional ASE noise significantly limited the capability of DDLMS, and the proposed algorithm gives the best performance with a GMI gain of at least 0.35 bit/4-D symbol compared with other equalization techniques. The
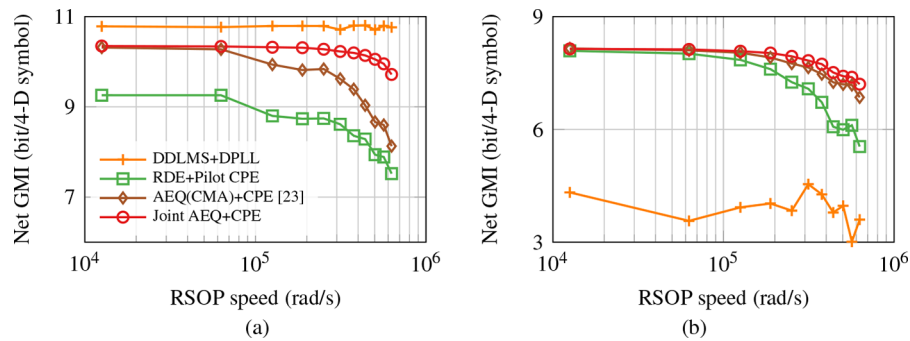
Fig. 9. Net GMI as a function of RSOP speed with different equalization and CPE algorithms in 56 GBaud 64 QAM transmission experiment. (a) Distance = 80 km; (b) Distance = 400 km.

experimental result shows that our proposed joint equalization and CPE scheme has a robust RSOP tracking performance under different OSNR conditions.

5. Conclusion

We have presented a pilot-based MIMO equalizer which achieves robust RSOP tracking and mitigates the PMD impairment, and demonstrated its effectiveness in a 56 GBaud PDM-64 QAM transmission system. The introduction of pilot symbols ensures the algorithm is immune to cycle slips, which is one of the main limitations of the blind DSP. The proposed method was numerically and experimentally compared to other adaptive equalization and carrier phase estimation algorithms proposed previously in the literature, namely the blind DDLMS and DPLL algorithm, RDE algorithm, and pilot symbol-based CMA. The results show that the proposed joint equalization and CPE achieves at least 0.35 bit per symbol higher generalized mutual information rate when tracking 600 krad/s RSOP after 400 km transmission. In addition, it is low-complexity and introduces minimal-delay in operation. Compared with other DSP algorithms, the robustness of the proposed scheme ensures that it can work under extreme conditions, such as low OSNR of 26 dB, fast RSOP speed of 600 krad/s, and broad laser linewidths of up to 2 MHz.

Disclosures. The authors declare no conflicts of interest.

Data availability. Data underlying the results presented in this paper are not publicly available at this time but may be obtained from the authors upon reasonable request.

References

1. S. J. Savory, "Digital coherent optical receivers: Algorithms and subsystems," IEEE J. Sel. Top. Quantum Electron. **16**(5), 1164–1179 (2010).
2. S. J. Savory, "Digital coherent optical access networks," in *2013 IEEE Photonics Conference*, (IEEE, 2013), pp. 125–126.
3. D. A. Morero, M. A. Castrillon, A. Aguirre, M. R. Hueda, and O. E. Agazzi, "Design tradeoffs and challenges in practical coherent optical transceiver implementations," J. Lightwave Technol. **34**(1), 121–136 (2016).
4. D. Rafique, H. Griesser, and J.-P. Elbers, "Enabling 64Gbaud coherent optical transceivers," in *2017 Optical Fiber Communications Conference and Exhibition (OFC)*, (IEEE, 2017), pp. 1–3.
5. S. J. Savory, "Digital filters for coherent optical receivers," Opt. Express **16**(2), 804–817 (2008).
6. K. Kikuchi, "Performance analyses of polarization demultiplexing based on constant-modulus algorithm in digital coherent optical receivers," Opt. Express **19**(10), 9868–9880 (2011).
7. M. S. Faruk and K. Kikuchi, "Adaptive frequency-domain equalization in digital coherent optical receivers," Opt. Express **19**(13), 12789–12798 (2011).

8. M. Morsy-Osman, M. Chagnon, Q. Zhuge, X. Xu, M. E. Mousa-Pasandi, Z. A. El-Sahn, and D. V. Plant, "Ultrafast and low overhead training symbol based channel estimation in coherent M-QAM single-carrier transmission systems," Opt. Express **20**(26), B171–B180 (2012).

9. R. Corsini, A. Peracchi, E. Matarazzo, T. Foggi, J. Nijhof, G. Meloni, L. Potì, R. Magri, and E. Ciaramella, "Blind adaptive chromatic dispersion compensation and estimation for DSP-based coherent optical systems," J. Lightwave Technol. **31**(13), 2131–2139 (2013).

10. K. Matsuda, R. Matsumoto, and N. Suzuki, "Hardware-efficient adaptive equalization and carrier phase recovery for 100-Gb/s/λ-based coherent WDM-PON systems," J. Lightwave Technol. **36**(8), 1492–1497 (2018).

11. X. Zhang, X. Li, T. Zeng, L. Meng, J. Li, M. Luo, F. Jiang, Z. Liu, and S. Yu, "Real time low-complexity adaptive channel equalization for coherent optical transmission systems," Opt. Express **28**(4), 5058–5068 (2020).

12. I. Fatadin, D. Ives, and S. J. Savory, "Blind equalization and carrier phase recovery in a 16-QAM optical coherent system," J. Lightwave Technol. **27**(15), 3042–3049 (2009).

13. Y. Mori, C. Zhang, and K. Kikuchi, "Novel configuration of finite-impulse-response filters tolerant to carrier-phase fluctuations in digital coherent optical receivers for higher-order quadrature amplitude modulation signals," Opt. Express **20**(24), 26236–26251 (2012).

14. R. G. van Uden, C. M. Okonkwo, V. A. Sleiffer, H. de Waardt, and A. M. Koonen, "MIMO equalization with adaptive step size for few-mode fiber transmission systems," Opt. Express **22**(1), 119–126 (2014).

15. D. Charlton, S. Clarke, D. Doucet, M. O'Sullivan, D. L. Peterson, D. Wilson, G. Wellbrock, and M. Bélanger, "Field measurements of SOP transients in OPGW, with time and location correlation to lightning strikes," Opt. Express **25**(9), 9689–9696 (2017).

16. S. M. Pietralunga, J. Colombelli, A. Fellegara, and M. Martinelli, "Fast polarization effects in optical aerial cables caused by lightning and impulse current," IEEE Photonics Technol. Lett. **16**(11), 2583–2585 (2004).

17. P. M. Krummrich, D. Ronnenberg, W. Schairer, D. Wienold, F. Jenau, and M. Herrmann, "Demanding response time requirements on coherent receivers due to fast polarization rotations caused by lightning events," Opt. Express **24**(11), 12442–12457 (2016).

18. Y. Yang, G. Cao, K. Zhong, X. Zhou, Y. Yao, A. P. T. Lau, and C. Lu, "Fast polarization-state tracking scheme based on radius-directed linear kalman filter," Opt. Express **23**(15), 19673–19680 (2015).

19. Q. Xiang, Y. Yang, Q. Zhang, and Y. Yao, "Low complexity, modulation-transparent and joint polarization and phase tracking scheme based on the nonlinear principal component analysis," Opt. Express **27**(13), 17968–17978 (2019).

20. T. Zeng, Z. He, L. Meng, J. Li, X. Li, and S. Yu, "The real time implementation of a simplified 2-section equalizer with supernal SOP tracking capability," in *Optical Fiber Communication Conference*, (Optical Society of America, 2020), pp. M2J–7.

21. P. Yi, D. Li, H. Song, M. Cheng, D. Liu, and L. Deng, "Experimental investigation on low-complexity adaptive equalizer including RSOP tracking and phase recovery for 112 Gb/s PDM-QPSK transmission system," IEEE Photonics J. **13**(2), 1–15 (2021).

22. M. Mazur, J. Schröder, A. Lorences-Riesgo, T. Yoshida, M. Karlsson, and P. A. Andrekson, "Overhead-optimization of pilot-based digital signal processing for flexible high spectral efficiency transmission," Opt. Express **27**(17), 24654–24669 (2019).

23. Y. Wakayama, E. Sillekens, L. Galdino, D. Lavery, R. I. Killey, and P. Bayvel, "Increasing achievable information rates with pilot-based DSP in standard intradyne detection," in *45th European Conference on Optical Communication (ECOC 2019)*, (IET, 2019), pp. 1–4.

24. W. Yi, E. Sillekens, D. Lavery, H. Dzieciol, S. Zhou, K. Law, J. Chen, P. Bayvel, and R. I. Killey, "Performance of momentum-based frequency-domain MIMO equalizer in the presence of feedback delay," Opt. Express **28**(13), 19133–19143 (2020).

25. B. Farhang-Boroujeny, *Adaptive filters: theory and applications* (John Wiley & Sons, 2013), 2nd ed.

26. E. Ip and J. M. Kahn, "Feedforward carrier recovery for coherent optical communications," J. Lightwave Technol. **25**(9), 2675–2692 (2007).

27. A. Spalvieri and L. Barletta, "Pilot-aided carrier recovery in the presence of phase noise," IEEE Trans. Commun. **59**(7), 1966–1974 (2011).

28. Y. Wakayama, T. Gerard, E. Sillekens, L. Galdino, D. Lavery, R. I. Killey, and P. Bayvel, "2048-QAM transmission at 15 GBd over 100 km using geometric constellation shaping," Opt. Express **29**(12), 18743–18759 (2021).

29. S. Camatel and V. Ferrero, "Narrow linewidth CW laser phase noise characterization methods for coherent transmission system applications," J. Lightwave Technol. **26**(17), 3048–3055 (2008).

30. T. Pfau, S. Hoffmann, and R. Noé, "Hardware-efficient coherent digital receiver concept with feedforward carrier recovery for *M*-qam constellations," J. Lightwave Technol. **27**(8), 989–999 (2009).